

Reevaluation of the hadronic vacuum polarisation contributions to the Standard Model predictions of the muon $g - 2$ and $\alpha(m_Z^2)$ using newest hadronic cross-section data

M. Davier¹, A. Hoecker², B. Malaescu³, and Z. Zhang¹

¹ Laboratoire de l'Accélérateur Linéaire, IN2P3-CNRS et Université Paris-Sud 11, F-91898, Orsay Cedex, France

² CERN, CH-1211, Geneva 23, Switzerland

³ Laboratoire de Physique Nucléaire et des Hautes Energies, IN2P3-CNRS et Universités Pierre-et-Marie-Curie et Denis-Diderot, F-75252 Paris Cedex 05, France

Abstract. We reevaluate the hadronic vacuum polarisation contributions to the muon magnetic anomaly and to the running of the electromagnetic coupling constant at the Z -boson mass. We include newest $e^+e^- \rightarrow$ hadrons cross-section data (among others) from the BABAR and VEPP-2000 experiments. For the muon $(g - 2)/2$ we find for the lowest-order hadronic contribution $(693.1 \pm 3.4) \cdot 10^{-10}$, improving the precision of our previous evaluation by 21%. The full Standard Model prediction differs by 3.5σ from the experimental value. The five-quark hadronic contribution to $\alpha(m_Z^2)$ is evaluated to be $(276.0 \pm 0.9) \cdot 10^{-4}$.

1 Introduction

The Standard Model (SM) predictions of the anomalous magnetic moment of the muon, $a_\mu = (g_\mu - 2)/2$, with g_μ the muon gyromagnetic factor, and of the running electromagnetic coupling constant, $\alpha(s)$, a crucial ingredient of electroweak theory, are limited in precision by hadronic vacuum polarisation (HVP) contributions. The dominant hadronic terms can be calculated with a combination of experimental cross-section data, involving e^+e^- annihilation to hadrons, and perturbative QCD. They are used to evaluate energy-squared dispersion integrals ranging from the $\pi^0\gamma$ threshold to infinity. The kernels occurring in these integrals emphasise low photon virtualities, owing to the $1/s$ descent of the cross section, and, in case of a_μ , to an additional $1/s$ suppression. In the latter case, about 73% of the lowest order hadronic contribution and 59% of the total uncertainty-squared are given by the $\pi^+\pi^-(\gamma)$ final state,¹ while this channel amounts to only 12% of the hadronic contribution to $\alpha(s)$ at $s = m_Z^2$.

In this work, we reevaluate the lowest-order hadronic contribution, $a_\mu^{\text{had,LO}}$, to the muon magnetic anomaly, and the hadronic contribution, $\Delta\alpha_{\text{had}}(m_Z^2)$, to the running $\alpha(m_Z^2)$ at the Z -boson mass using newest $e^+e^- \rightarrow$ hadrons cross-section data. The BABAR Collaboration has essentially completed a programme of precise measurements of exclusive hadronic cross sections for all the dominant channels from threshold to an energy of 3–5 GeV using the initial-state radiation (ISR) method. Also new results are being produced at the VEPP-2000 facility in Novosibirsk, Russia in the 1–2 GeV energy

range. The new data complement the available information on exclusive channels allowing to alleviate the need for estimating missing channels with the use of isospin symmetry.

We reevaluate all the experimental contributions using the software package HVPTools [1], and add to these narrow resonance contributions evaluated analytically and continuum contributions obtained from perturbative QCD.

2 Input data

Exclusive bare hadronic cross-section measurements are integrated up to 1.8 GeV over the relevant dispersion kernels. In the present work 39 channels are included, as compared to only 22 in our latest work from 2011 [2]. Thanks to the new measurements only very few final states remain to be estimated using isospin symmetry. In the energy range 1.8–3.7 GeV and above 5 GeV four-loop perturbative QCD is used [3]. The contributions from the open charm pair production region between 3.7 and 5 GeV are again computed using experimental data. For the narrow resonances J/ψ and $\psi(2S)$ Breit-Wigner line shapes are integrated using their currently best known parameters.

The integration of data points belonging to different experiments with their own data densities requires a careful treatment especially with respect to correlated systematic uncertainties within the same experiment and between different experiments. Quadratic interpolation of adjacent data points is performed for each experiment and a local combination between the interpolations is computed in bins of 1 MeV. Full covariance matrices are constructed between experiments and

¹ Throughout this paper, final state photon radiation is implied for all hadronic final states.

channels. Uncertainties are propagated using pseudo-experiment generation and closure tests with known distributions are performed to validate both the combination and integration. Where results from different experiments are locally inconsistent the combined uncertainty is rescaled according to the local χ^2 value following the well-known PDG approach. At present, for the dominant $\pi^+\pi^-$ channel such inconsistencies are limiting the precision of the combination. In most exclusive channels the largest weight in the combination is provided by BABAR measurements.

The following channel-wise discussion focuses on the HVP contribution to a_μ as it stronger relies on the low-energy experimental data. We mainly explore the impact of the data released since our last publication [2], which provides references to all the older datasets used in the combination.

2.1 The dominant $\pi^+\pi^-$ channel

The $\pi^+\pi^-$ channel dominates both the HVP contribution to a_μ and its uncertainty. Recent experiments are generally limited by systematic uncertainties. The main contributors are BABAR [4, 5] (relative systematic uncertainty of 0.5% per measurement), KLOE-2008 [6] (0.8%), KLOE-2010 [7] (1.4%), CMD2 [10, 11] (0.8%), and SND [12] (1.5%). For this update we newly included KLOE-2012 [8] (0.8%) and the recent BESIII-2015 [9] (0.9%). Only BABAR covers the full $\pi^+\pi^-$ mass range with high precision.

The three KLOE measurements exhibit statistical correlations due to the common two-pion events used in the 2008 and 2012 results (the 2012 analysis uses the pion over muon pair cross-section ratio), and systematic correlations from common uncertainty sources.²

Figure 1 shows the available $e^+e^- \rightarrow \pi^+\pi^-$ cross-section measurements in various panels zooming into different centre-of-mass energies (\sqrt{s}). The green band indicates the HVPTools combination within its 1σ uncertainty. The deviations between the combination and the most precise individual measurements are plotted in Fig. 2. Figure 3 (left) shows the local combination weight versus \sqrt{s} per experiment. The BABAR and KLOE measurements dominate over the entire energy

² Correlations due to systematic uncertainties among the three KLOE datasets are accounted for by matching one-by-one the uncertainties impacting the measurements. For example, the uncertainties due to the luminosity, radiator function and vacuum polarisation are taken to be correlated among the first two measurements, while they are found negligible or not present in the 2012 measurement. The final state radiation uncertainty as well as the trigger, tracking, acceptance and background uncertainties for the $\pi\pi$ data are taken to be correlated among the three measurements, while the background uncertainty for the $\mu\mu$ data only impacts the 2012 measurement. We will replace this approximate treatment by a more accurate one once it is provided by the KLOE Collaboration.

range. Owing to the sharp radiator function, the event yield increases for KLOE towards the $\phi(1020)$ mass, hence outperforming BABAR above ~ 0.8 GeV. The group of experiments labelled ‘‘Other exp’’ in Fig. 3 corresponds to older data with incomplete radiative corrections. Their weights are small throughout the entire energy domain. The computation of the dispersion integral over the full $\pi^+\pi^-$ spectrum requires to extend the available data to the region between threshold and 0.3 GeV, for which we use a fit as described in Ref. [1].

A tension between the BABAR and KLOE measurements is observed at and above the $\rho(770)$ peak region (cf. Fig. 2), while the other measurements are consistent with both. We stress the importance of locally assessing the compatibility of the (correlated) cross-section measurements, rather than comparing integrated values where discrepancies could cancel or be diluted. The local uncertainty rescaling we apply (cf. right-hand plot of Fig. 3) increases the combined $a_\mu^{\text{had,LO}}$ uncertainty by 15% in the $\pi^+\pi^-$ channel.

In spite of this problem, progress in the evaluation of the $\pi^+\pi^-$ contribution to $a_\mu^{\text{had,LO}}$ has been steady during the last decade. While the central value stayed within quoted uncertainties, the uncertainty dropped from³ 5.9 in 2003 to 2.8 in 2011, and now amounts to 2.6. The updated contribution from threshold to 1.8 GeV is $507.1 \pm 1.1 \pm 2.2 \pm 0.8$, where the first uncertainty is statistical, and the second and third stand for systematic uncertainties that are, respectively, uncorrelated and correlated with other channels. The correlation originates mainly from uncertainties in the luminosity and in radiative corrections, most notably the vacuum polarisation correction applied to the measured cross sections.

Our $a_\mu^{\text{had,LO}}$ ($\pi^+\pi^-$) estimate using $\tau^- \rightarrow \pi^-\pi^0\nu_\tau$ data from ALEPH, OPAL, CLEO, and Belle, $516.2 \pm 2.9 \pm 2.2$ [13], where the first uncertainty is experimental and the second due to isospin-breaking corrections, is 2.0σ larger than the current e^+e^- -based value. The difference can be reduced by applying off-resonance γ - ρ mixing corrections [14] that come with additional uncertainties. Because of the progress in the e^+e^- data, the τ input is now less precise and less reliable due to additional theoretical uncertainties. While the τ versus e^+e^- comparison is interesting in its own right, we do no longer consider the τ data for the HVP evaluation.

2.2 The $\pi^+\pi^-\pi^0$ channel

Following the treatment described in Ref. [2] the contributions from $\omega(782)$ and $\phi(1020)$ decaying to three pions are directly evaluated from the $e^+e^- \rightarrow \pi^+\pi^-\pi^0$ cross-section measurements (cf. Fig. 4). Other resonant decays are included in the corresponding $\pi^0\gamma$, $\eta\gamma$, and

³ Unless specified, these and all other a_μ related values throughout this paper are given in units of 10^{-10} .

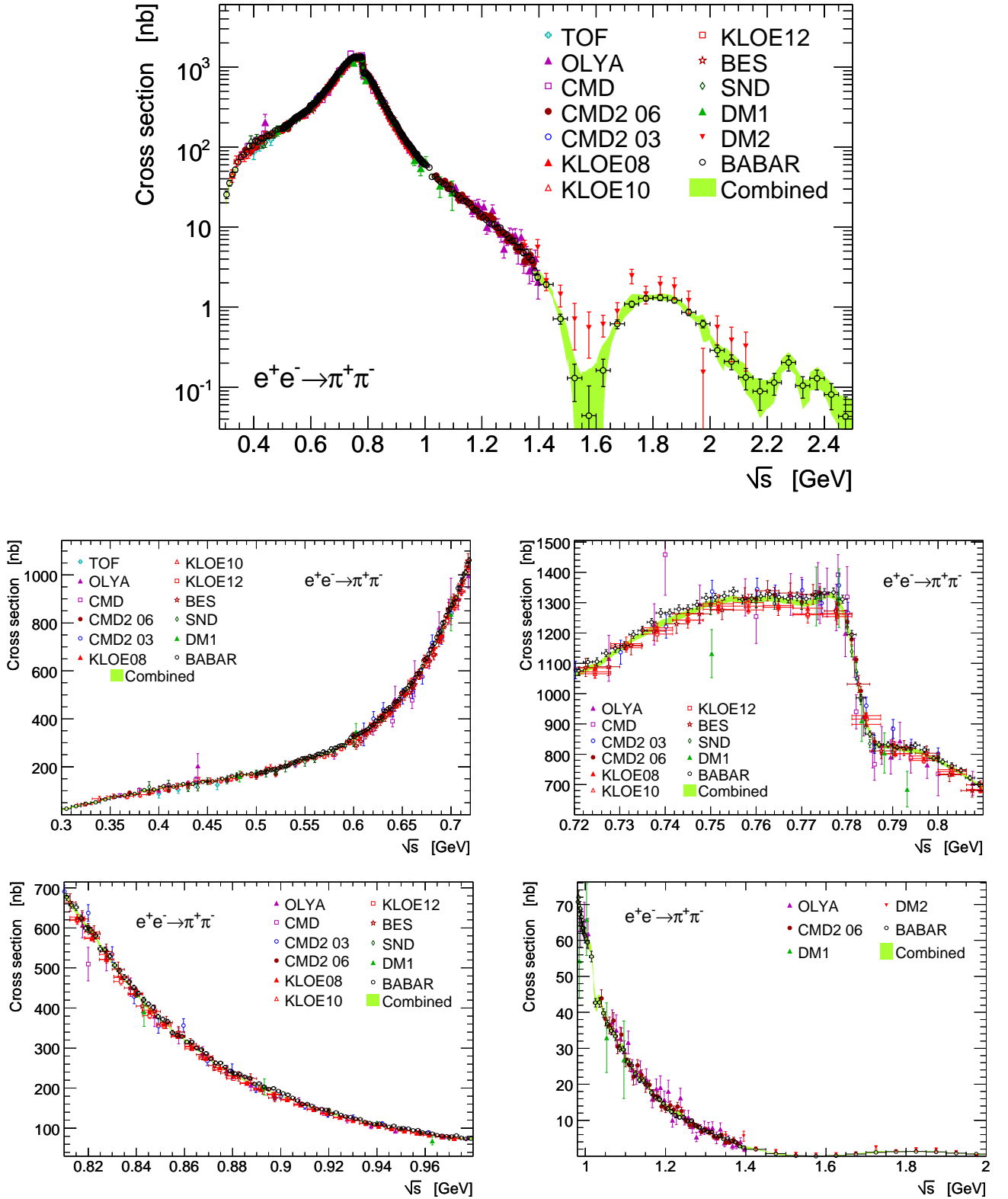


Fig. 1. Bare cross section of $e^+e^- \rightarrow \pi^+\pi^-$ versus centre-of-mass energy for different energy ranges. The error bars of the data points include statistical and systematic uncertainties added in quadrature. The green band shows the HVPTools combination within its 1σ uncertainty.

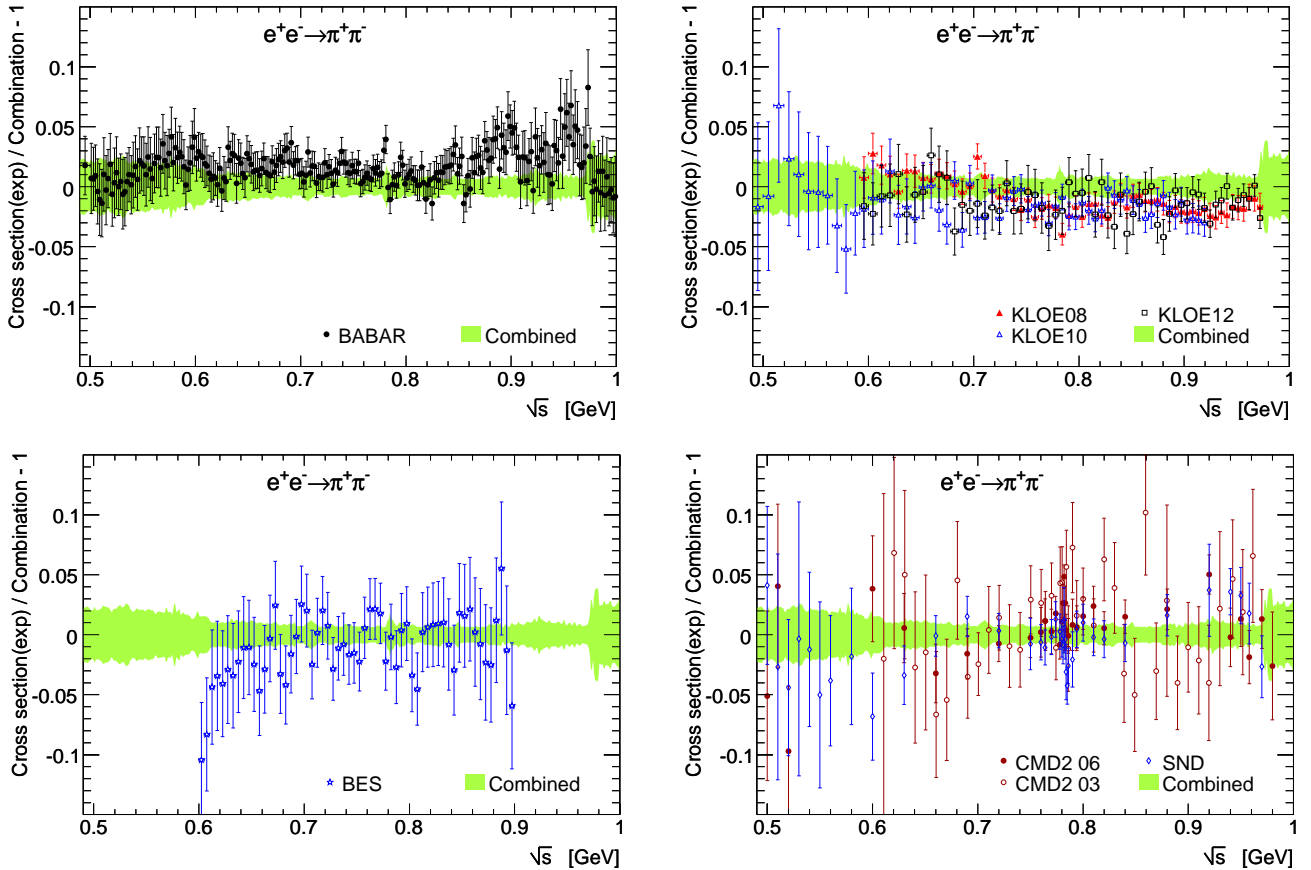


Fig. 2. Comparison between individual $e^+e^- \rightarrow \pi^+\pi^-$ cross-section measurements from BABAR [4, 5], KLOE08 [6], KLOE10 [7], KLOE12 [8], BESIII [9], CMD2 03 [10], CMD2 06 [11], SND [12], and the HVPTools combination. The error bars include statistical and systematic uncertainties added in quadrature.

$K\bar{K}$ spectra, while small remaining non-resonant decay modes are considered separately.

2.3 The four-pion channels

Recent results using the full BABAR data on $e^+e^- \rightarrow \pi^+\pi^-2\pi^0$ are now available [15]. As with other BABAR measurements using the ISR method with the ISR photon measured at large angle, the acceptance for the recoiling hadronic system is large so that the resonance substructure, dominated by the $\omega\pi^0$, $\rho^0\pi^0\pi^0$, and $\rho^+\rho^-$ final states, can be fully identified and accurately modelled with a Monte Carlo generator. The systematic uncertainty is 3.1% below 2.7 GeV, a considerable improvement over the value of about 10% of preliminary results available so far. Data from some older experiments, both imprecise and inconsistent, are now discarded. As seen in the left hand plot of Fig. 5 the BABAR results lead to a substantial precision improvement in this channel.

The $\pi^+\pi^-2\pi^0$ HVP contribution to $a_\mu^{\text{had,LO}}$ from threshold to 1.8 GeV is $18.03 \pm 0.06 \pm 0.48 \pm 0.26$, where the total uncertainty of 0.55 is reduced by a factor of

2.3 compared to our 2011 result [2]. We note that the τ -based result $21.0 \pm 1.2 \pm 0.4$ (the second uncertainty accounts for isospin-symmetry breaking corrections), obtained from a combination of $\nu_\tau\pi^-\pi^+\pi^-$ and $\nu_\tau\pi^-3\pi^0$ spectral functions measured by ALEPH [13], is 2.2σ larger than the e^+e^- value and twice less precise.

New $2\pi^+2\pi^-$ cross-section data (cf. right hand plot in Fig. 5) were published by BABAR in 2012 [16] using the full available data sample and with a reduced systematic uncertainty (2.4%) compared to previous partial results. New measurements from CMD3 between 0.920 and 1.060 GeV are also available [17]. The resulting combined HVP contribution is $13.68 \pm 0.03 \pm 0.27 \pm 0.14$, with a total uncertainty of 0.31 reduced by a factor of 1.7 compared to our 2011 result [2].

For comparison, the ALEPH τ -based prediction of $2\pi^+2\pi^-$, $12.8 \pm 0.7 \pm 0.4$ [13], is consistent, but more than twice less precise than the e^+e^- -based one. The τ -based evaluation of the sum of the two four-pion channels, 33.8 ± 1.5 , benefits from an anticorrelation due to the $\nu_\tau\pi^\pm 3\pi^0$ contribution in both channels. It is consistent with the e^+e^- -based value of 31.7 ± 0.6 within 1.3σ . The τ -based cross-section predictions are compared to the e^+e^- data in Fig. 5.

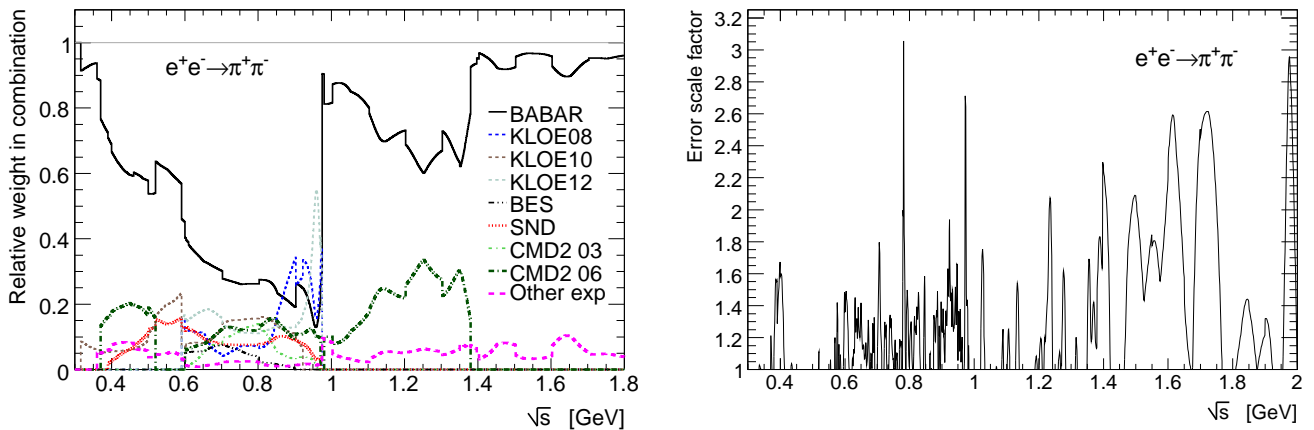


Fig. 3. Left: relative local weight per experiment contributing to the $e^+e^- \rightarrow \pi^+\pi^-$ cross-section combination versus centre-of-mass energy. Right: local scale factor versus centre-of-mass energy applied to the combined $\pi^+\pi^-$ cross-section uncertainty to account for inconsistency in the individual measurements.

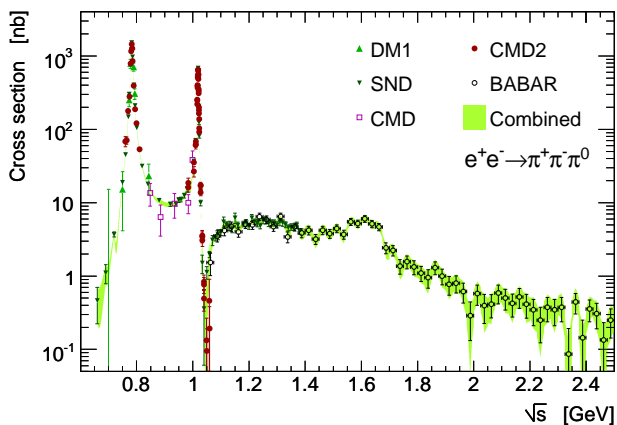


Fig. 4. Bare cross section of $e^+e^- \rightarrow \pi^+\pi^-\pi^0$ versus centre-of-mass energy. The error bars of the data points include statistical and systematic uncertainties added in quadrature. The green band shows the HVPTools combination within its 1σ uncertainty.

2.4 The $K\bar{K}$ channels

New cross-section measurements are available for the $K_S^0 K_L^0$ channel. The BABAR experiment detects both K_S^0 and K_L^0 from threshold up to 2.2 GeV [18], while CMD3 counts K_S^0 in the $\phi(1020)$ resonance region [19]. Consistency is observed between the two experiments as well as with older measurements from CMD2 and SND. The measured cross sections are shown in the right panel of Fig. 6.

The $K_S^0 K_L^0$ contribution to $a_\mu^{\text{had,LO}}$ up to 1.8 GeV amounts to $12.81 \pm 0.06 \pm 0.18 \pm 0.15$ with a total uncertainty of 0.24, which is reduced by a factor of 1.6 over that of our 2011 estimate [2].

Recent measurements from SND [20] at VEPP-2000 for the K^+K^- channel agree with BABAR [21], while both show a discrepancy with former SND data, obtained at VEPP-2M below 1.4 GeV, that exceeds the

quoted systematic uncertainty. The BABAR and new SND data are displayed in the left hand panel of Fig. 6.

Some concern arises with regard to the $e^+e^- \rightarrow \phi \rightarrow K^+K^-$ cross-section measurements. The BABAR result has a systematic uncertainty of 0.7%, but it is larger by 5.1% (9.6%) than CMD2 (SND) which has a systematic uncertainty of 2.2% (7.1%). Including the BABAR data the contribution to $a_\mu^{\text{had,LO}}$ increases from 21.63 to 22.67 with an uncertainty of 0.43. A recent preliminary result from CMD3 [22] shows a very large ($\sim 11\%$) excess of the cross section over CMD2 and $\sim 5\%$ over BABAR. The origin of this large discrepancy is not understood at present [23]. It raises doubts on the ability to perform a precision measurement of this channel with the standard energy-scan method because the detection efficiency of the low-momentum K^\pm from ϕ decay is difficult to model. Owing to the boost of the final state, the ISR method is expected to be more reliable for the charged kaon detection.

2.5 The $K\bar{K}$ + pions channels

In previous hadronic vacuum polarisation analyses the available exclusive $e^+e^- \rightarrow K\bar{K} + \text{pions}$ data were incomplete. Missing channels were constrained based on assumptions about the process dynamics and isospin symmetry [24, 2] leading to considerable uncertainty. This procedure became unnecessary since the BABAR experiment produced cross-section results for the three channels contributing to the final state $K\bar{K}\pi$ and six channels contributing to $K\bar{K}\pi\pi$. A key ingredient of the BABAR analyses is the detection of neutral kaons, both K_S^0 , through the $\pi^+\pi^-$ decay, and K_L^0 interacting in the calorimeters.

Together with previous measurements of $K_S^0 K^\pm \pi^\mp$ and $K^+ K^- \pi^0$, data for $K_S^0 K_L^0 \pi^0$ [25] complete the picture for the $K\bar{K}\pi$ channel (cf. top row panels in Fig. 7). Because that final state is dominated by $K^* \bar{K}$ produc-

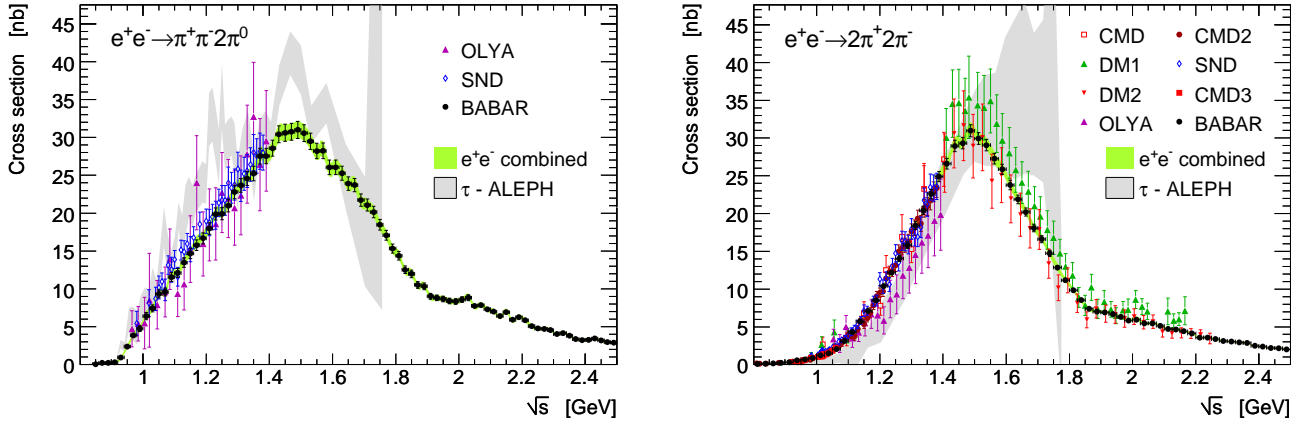


Fig. 5. Bare cross sections for $e^+e^- \rightarrow \pi^+\pi^-2\pi^0$ (left) and $e^+e^- \rightarrow 2\pi^+2\pi^-$ (right). The error bars of the data points include statistical and systematic uncertainties added in quadrature. The green bands show the HVPTools combinations within 1σ uncertainties. The cross-section predictions within 1σ uncertainties derived from ALEPH τ four-pion spectral functions are indicated by the light grey bands.

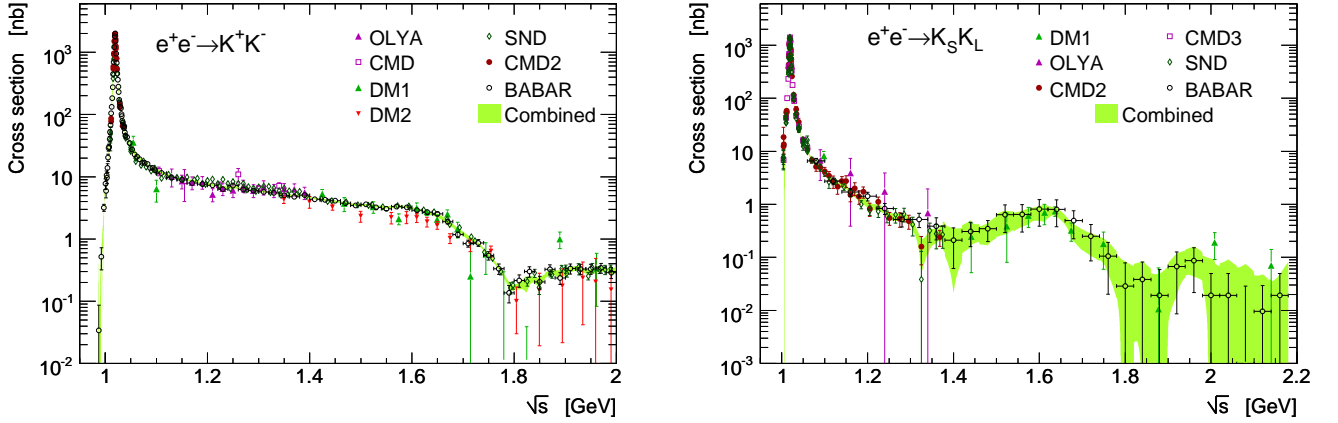


Fig. 6. Bare cross sections for $e^+e^- \rightarrow K^+K^-$ (left) and $e^+e^- \rightarrow K_S^0K_L^0$ (right). See text for a description of the data used.

tion below 1.8 GeV (with a small contribution from $\phi\pi^0$), it is expected that isospin symmetry provides a good approximation. Indeed, the contribution from the sum of the measured channels, 2.45 ± 0.15 , is in agreement with and has similar precision as the result 2.39 ± 0.16 obtained from the $K_S^0K^\pm\pi^\mp$ data only together with isospin symmetry.

Of the six channels contributing to $K\bar{K}\pi\pi$ only two, $K^+K^-\pi^+\pi^-$ and $K^+K^-2\pi^0$, had been measured by BABAR in 2011. Constraints from isospin symmetry were used to estimate the missing channels [2], but because of the complex dynamics involving $K^*(890)\bar{K}\pi$, $K\bar{K}\rho$ and $\phi\pi\pi$ intermediate states, these estimates were plagued by substantial uncertainties. Among the remaining channels, $K_S^0K_L^0\pi^+\pi^-$ [18], $K_S^0K_S^0\pi^+\pi^-$ [18], $K_S^0K_L^02\pi^0$ [25], and $K_S^0K^\pm\pi^\pm\pi^0$ [26] have been measured by BABAR. In addition, the previously measured channels $K^+K^-\pi^+\pi^-$ and $K^+K^-2\pi^0$ have been updated with the full data sample [27]. New measurements

of $K^+K^-\pi^+\pi^-$ became available from CMD3 [28] and are in agreement with the BABAR data. Except for $K_L^0K_L^0\pi^+\pi^-$, which can be safely estimated using CP symmetry, all cross sections have now been measured.

The precision in the inclusive contribution to $a_\mu^{\text{had,LO}}$ from all $K\bar{K}\pi\pi$ final states improved from previously 0.39, dominated by the uncertainty in the estimates from isospin symmetry [2], to presently 0.05 (cf. Table 1 on page 9).

2.6 Other channels

Data on many processes with smaller cross sections, mainly from VEPP-2000, have become available and are included in the HVPTools database. This is the case for $3\pi^+3\pi^-$ from CMD3 [29], $\pi^0\gamma$ [30], $\eta\gamma$ [31], $\eta\pi^+\pi^-$ [32], and $\omega\pi^0$ [33] from SND, $\eta\omega$ from SND [34] and CMD3 [35], nonresonant $\eta\pi^+\pi^-\pi^0$ from CMD3 [35], $\eta\pi^+\pi^-$ from BABAR [36], which extend and improve

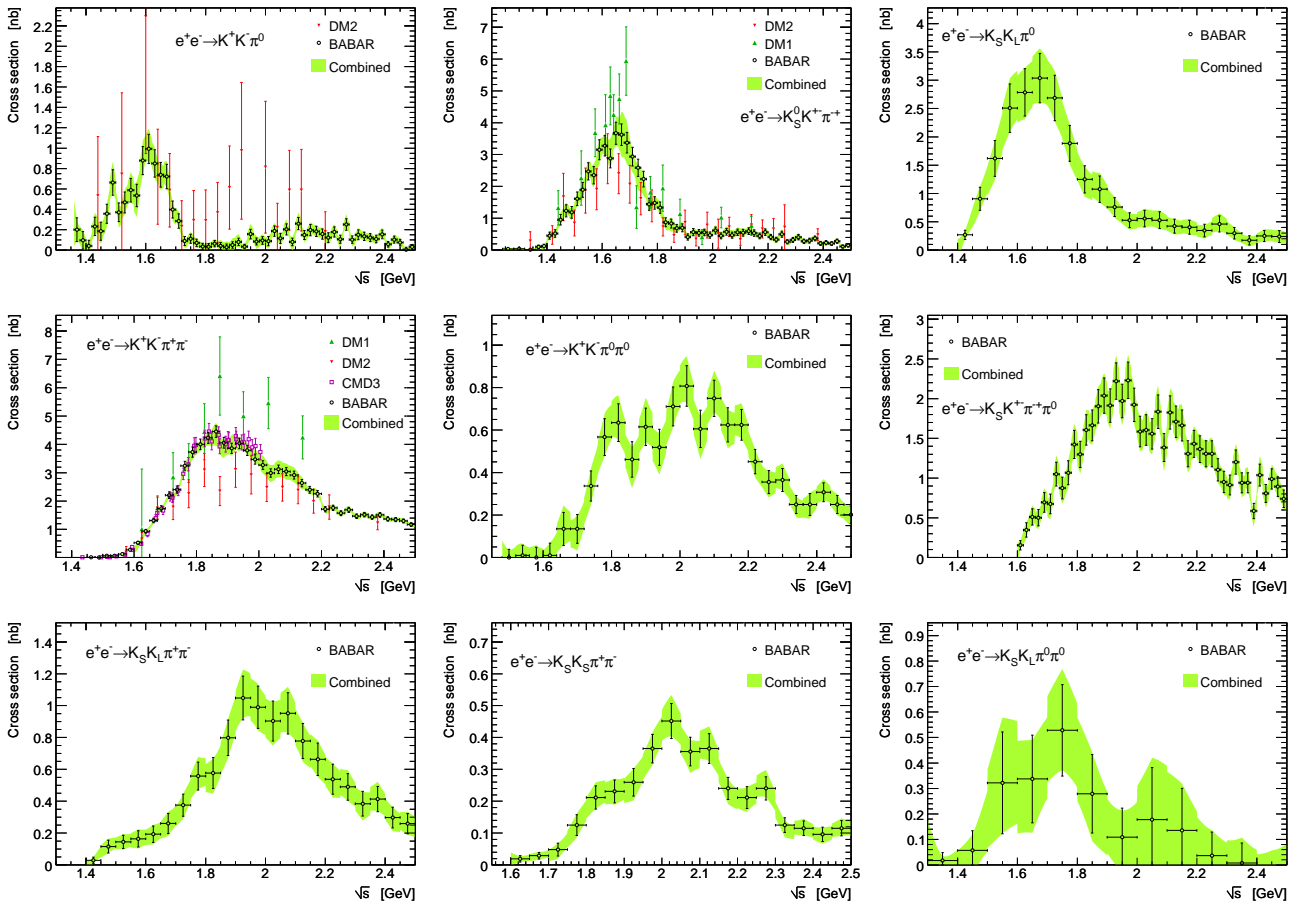


Fig. 7. Bare cross-section data for $K\bar{K}\pi$ (top row) and $K\bar{K}\pi\pi$ (middle and bottom rows) final states. See text for references. The error bars of the data points include statistical and systematic uncertainties added in quadrature. The green bands show the HVPTools interpolations within 1σ uncertainties. Because the integral of the interpolation within a bin of a given measurement is rescaled to equal the bin content (recall that the BABAR cross-section measurements are obtained from unfolded histograms) the interpolated cross section can appear slightly shifted with respect to the measurement in cases of local shape variations.

older measurements in these channels. Except for the $\eta\omega$ cross section above 1.6 GeV, results using the ISR technique at BABAR and the scan method at VEPP-2000 are in agreement notwithstanding their different systematic uncertainties. Above 1.8 GeV the production of $p\bar{p}$ measured by BABAR [37] and CMD3 [38], $n\bar{n}$ by ADONE [39] and SND [40], and $\eta\omega\pi^0$ by SND [41] are included.

Figure 8 shows the available measurements and their combination of the charm resonance region above the opening of the $D\bar{D}$ channel. The individual datasets agree within uncertainties. While Crystal Ball [45] and BES [42] published bare inclusive cross-section results, PLUTO applied only radiative corrections [46] following the formalism of Ref. [47], which does not include HVP. Following similar previous cases [48], we have applied this correction and assigned a 50% systematic uncertainty to it.

2.7 Estimated missing channels

Even with the large number of exclusive cross-section measurements available below 2 GeV, covering particle multiplicities up to six hadrons including π^0 and η mesons, a few channels with more than two neutral pions are still unmeasured and their contributions must be estimated using isospin symmetry. The treatment of the channels $\pi^+\pi^-3\pi^0$, $\pi^+\pi^-4\pi^0$, and $\eta\pi^+\pi^-2\pi^0$ follows our previous approach detailed in Ref. [2].

Whereas the $e^+e^- \rightarrow \eta\phi$ cross-section data were already included, the previously neglected smaller contribution from $e^+e^- \rightarrow \eta(K^+K^-)_{\text{non-}\phi}$ where the K^+K^- does not originate from resonant ϕ decay is now taken into account following a BABAR measurement [49]. Its unmeasured counterpart $e^+e^- \rightarrow \eta(K_S K_L)_{\text{non-}\phi}$ can be crudely estimated to equal the corresponding K^+K^- contribution with a 100% systematic uncertainty. This estimate is consistent with the upper limit that can be deduced using BABAR's $K_S^0 K_L^0 \eta$ measurement [25].

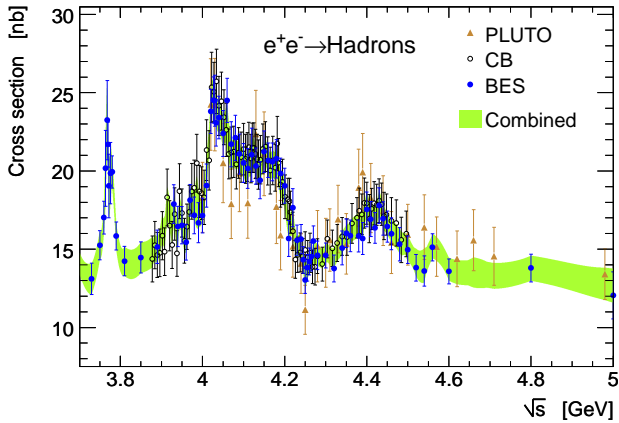


Fig. 8. Inclusive bare hadronic cross section versus centre-of-mass energy above the $D\bar{D}$ threshold. The error bars of the data points include statistical and systematic uncertainties added in quadrature. The green band shows the HVPTools combination within its 1σ uncertainty.

Altogether the contribution from missing channels to $a_\mu^{\text{had,LO}}$ up to 1.8 GeV is estimated to be 0.46 ± 0.12 , corresponding to a fraction of only $(0.09 \pm 0.02)\%$ of the full HVP contribution in this range. The corresponding fraction in our 2011 analysis was much larger, $(0.69 \pm 0.07)\%$, illustrating the experimental progress made.

3 Compilation and results

A compilation of the various contributions to $a_\mu^{\text{had,LO}}$ and to $\Delta\alpha_{\text{had}}(m_Z^2)$, as well as the total results are given in Table 1. The experimental uncertainties are separated into statistical, channel-specific systematic, and common systematic contributions that are correlated with at least one other channel.

The contributions from the J/ψ and $\psi(2S)$ resonances in Table 1 are obtained by numerically integrating the corresponding undressed⁴ Breit-Wigner line-shapes.⁵ The uncertainties in the integrals are dominated by the knowledge of the corresponding bare electronic width $\Gamma_{R \rightarrow ee}^0$ for which we use the values 5.60 ± 0.06 keV for $R = J/\psi$ [51] and 2.35 ± 0.05 keV for $R = \psi(2S)$ [52].

Sufficiently far from the quark thresholds we use four-loop [53] perturbative QCD, including $\mathcal{O}(\alpha_s^2)$ quark mass corrections [54], to compute the inclusive hadronic cross section. Nonperturbative contributions at 1.8 GeV were determined from data [55] and found to be small. The uncertainties of the R_{QCD} contributions given in

⁴ The undressing uses the BABAR programme AFKVAC correcting for both leptonic and hadronic VP effects. The correction factors amount to $(1 - \Pi(s))^2 = 0.956$ and 0.957 for the J/ψ and $\psi(2S)$, respectively.

⁵ Using instead the narrow-width approximation, $\sigma_R = 12\pi^2 \Gamma_{ee}^0 / M_R \cdot \delta(s - M_R^2)$, gives consistent results.

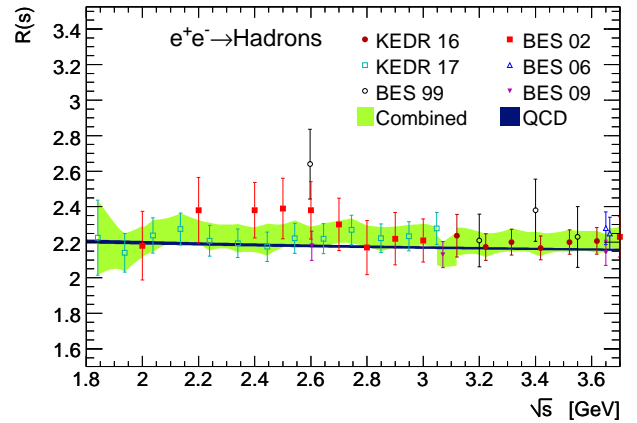


Fig. 9. Inclusive bare hadronic cross-section ratio versus centre-of-mass energy in the continuum region below the $D\bar{D}$ threshold. Shown are BES [42] and KEDR [43, 44] data points with statistical and systematic errors added in quadrature, the HVPTools combination (green band), and the prediction from perturbative QCD (dark blue line).

Table 1 are obtained from the quadratic sum of the uncertainty in α_s (we use $\alpha_s(m_Z^2) = 0.1193 \pm 0.0028$ from the fit to Z precision data [56]), the truncation of the perturbative series (we use the full four-loop contribution as systematic uncertainty), the difference between fixed-order perturbation theory and, so-called, contour-improved perturbation theory [57], as well as quark mass uncertainties (we use the values and uncertainties from Ref. [58]). The former three uncertainties are taken to be fully correlated between the various energy regions (see Table 1), whereas the (smaller) quark-mass uncertainties are taken to be uncorrelated.

The KEDR Collaboration has recently published results from an inclusive R scan from $\sqrt{s} = 1.84$ to 3.05 GeV [44], complementing their previous measurements obtained between 3.12 and 3.72 GeV [43]. These data are the most precise and complete in this energy range with a typical systematic uncertainty of 3% for a total of 20 measurements. They constitute a very valuable input to test the validity of the perturbative QCD estimate (cf. Fig. 9). Integrating the dispersion integrals between 2.0 and 3.7 GeV gives for the combined data 25.82 ± 0.61 ($a_\mu^{\text{had,LO}}$ in the usual units) and $(21.22 \pm 0.48) \cdot 10^{-4}$ ($\Delta\alpha_{\text{had}}(m_Z^2)$), compared to the QCD predictions 25.15 ± 0.19 and $(20.69 \pm 0.14) \cdot 10^{-4}$, respectively. Agreement within 1σ is found.

To examine the transition region between the sum of exclusive measurements and QCD we have computed $a_\mu^{\text{had,LO}}$ and $\Delta\alpha_{\text{had}}(m_Z^2)$ in the narrow energy interval 1.8–2.0 GeV. For the former quantity we find 7.71 ± 0.32 and 8.30 ± 0.09 for data and QCD, respectively. The full difference of 0.59 ($0.26 \cdot 10^{-4}$ in the case of $\Delta\alpha_{\text{had}}(m_Z^2)$) is assigned as additional systematic uncertainty, labelled by “dual” subscripts in Table 1. It accounts for possible low-mass quark-hadron duality violation affecting the perturbative QCD approximation

| Channel | $a_\mu^{\text{had,LO}} [10^{-10}]$ | $\Delta\alpha_{\text{had}}(m_Z^2) [10^{-4}]$ |
|--|---|---|
| $\pi^0\gamma$ | $4.29 \pm 0.06 \pm 0.04 \pm 0.07$ | $0.35 \pm 0.00 \pm 0.00 \pm 0.01$ |
| $\eta\gamma$ | $0.65 \pm 0.02 \pm 0.01 \pm 0.01$ | $0.08 \pm 0.00 \pm 0.00 \pm 0.00$ |
| $\pi^+\pi^-$ | $507.14 \pm 1.13 \pm 2.20 \pm 0.75$ | $34.39 \pm 0.07 \pm 0.15 \pm 0.05$ |
| $\pi^+\pi^-\pi^0$ | $46.20 \pm 0.40 \pm 1.10 \pm 0.86$ | $4.60 \pm 0.04 \pm 0.11 \pm 0.08$ |
| $2\pi^+2\pi^-$ | $13.68 \pm 0.03 \pm 0.27 \pm 0.14$ | $3.58 \pm 0.01 \pm 0.07 \pm 0.03$ |
| $\pi^+\pi^-2\pi^0$ | $18.03 \pm 0.06 \pm 0.48 \pm 0.26$ | $4.45 \pm 0.02 \pm 0.12 \pm 0.07$ |
| $2\pi^+2\pi^-\pi^0$ (η excl.) | $0.69 \pm 0.04 \pm 0.06 \pm 0.03$ | $0.21 \pm 0.01 \pm 0.02 \pm 0.01$ |
| $\pi^+\pi^-3\pi^0$ (η excl., isospin) | $0.35 \pm 0.02 \pm 0.03 \pm 0.01$ | $0.11 \pm 0.01 \pm 0.01 \pm 0.00$ |
| $3\pi^+3\pi^-$ | $0.11 \pm 0.00 \pm 0.01 \pm 0.00$ | $0.04 \pm 0.00 \pm 0.00 \pm 0.00$ |
| $2\pi^+2\pi^-2\pi^0$ (η excl.) | $0.72 \pm 0.06 \pm 0.07 \pm 0.14$ | $0.25 \pm 0.02 \pm 0.02 \pm 0.05$ |
| $\pi^+\pi^-4\pi^0$ (η excl., isospin) | $0.11 \pm 0.01 \pm 0.11 \pm 0.00$ | $0.04 \pm 0.00 \pm 0.04 \pm 0.00$ |
| $\eta\pi^+\pi^-$ | $1.18 \pm 0.03 \pm 0.06 \pm 0.02$ | $0.34 \pm 0.01 \pm 0.02 \pm 0.01$ |
| $\eta\omega$ | $0.32 \pm 0.02 \pm 0.02 \pm 0.01$ | $0.10 \pm 0.01 \pm 0.01 \pm 0.00$ |
| $\eta\pi^+\pi^-\pi^0$ (non- ω, ϕ) | $0.39 \pm 0.03 \pm 0.11 \pm 0.03$ | $0.13 \pm 0.01 \pm 0.04 \pm 0.01$ |
| $\eta 2\pi^+2\pi^-$ | $0.03 \pm 0.01 \pm 0.00 \pm 0.00$ | $0.01 \pm 0.00 \pm 0.00 \pm 0.00$ |
| $\eta\pi^+\pi^-2\pi^0$ | $0.03 \pm 0.01 \pm 0.01 \pm 0.00$ | $0.01 \pm 0.00 \pm 0.00 \pm 0.00$ |
| $\omega\pi^0$ ($\omega \rightarrow \pi^0\gamma$) | $0.94 \pm 0.01 \pm 0.02 \pm 0.02$ | $0.20 \pm 0.00 \pm 0.00 \pm 0.00$ |
| $\omega(\pi\pi)^0$ ($\omega \rightarrow \pi^0\gamma$) | $0.08 \pm 0.00 \pm 0.01 \pm 0.00$ | $0.03 \pm 0.00 \pm 0.00 \pm 0.00$ |
| ω (non- $3\pi, \pi\gamma, \eta\gamma$) | $0.36 \pm 0.00 \pm 0.01 \pm 0.00$ | $0.03 \pm 0.00 \pm 0.00 \pm 0.00$ |
| K^+K^- | $22.81 \pm 0.24 \pm 0.28 \pm 0.17$ | $3.31 \pm 0.03 \pm 0.04 \pm 0.03$ |
| $K_S K_L$ | $12.82 \pm 0.06 \pm 0.18 \pm 0.15$ | $1.74 \pm 0.01 \pm 0.03 \pm 0.02$ |
| ϕ (non- $K\bar{K}, 3\pi, \pi\gamma, \eta\gamma$) | $0.05 \pm 0.00 \pm 0.00 \pm 0.00$ | $0.01 \pm 0.00 \pm 0.00 \pm 0.00$ |
| $K\bar{K}\pi$ | $2.45 \pm 0.06 \pm 0.12 \pm 0.07$ | $0.78 \pm 0.02 \pm 0.04 \pm 0.02$ |
| $K\bar{K}2\pi$ | $0.85 \pm 0.02 \pm 0.05 \pm 0.01$ | $0.30 \pm 0.01 \pm 0.02 \pm 0.00$ |
| $K\bar{K}3\pi$ (estimate) | $-0.03 \pm 0.01 \pm 0.02 \pm 0.00$ | $-0.01 \pm 0.00 \pm 0.01 \pm 0.00$ |
| $\eta\phi$ | $0.36 \pm 0.02 \pm 0.02 \pm 0.01$ | $0.13 \pm 0.01 \pm 0.01 \pm 0.00$ |
| $\eta K\bar{K}$ (non- ϕ) | $0.01 \pm 0.01 \pm 0.01 \pm 0.00$ | $0.00 \pm 0.00 \pm 0.01 \pm 0.00$ |
| $\omega K\bar{K}$ ($\omega \rightarrow \pi^0\gamma$) | $0.01 \pm 0.00 \pm 0.00 \pm 0.00$ | $0.00 \pm 0.00 \pm 0.00 \pm 0.00$ |
| $\omega\eta\pi^0$ | $0.06 \pm 0.04 \pm 0.00 \pm 0.00$ | $0.02 \pm 0.02 \pm 0.00 \pm 0.00$ |
| J/ψ (BW integral) | 6.28 ± 0.07 | 7.09 ± 0.08 |
| $\psi(2S)$ (BW integral) | 1.57 ± 0.03 | 2.50 ± 0.04 |
| $R_{\text{data}} [3.7\text{--}5.0 \text{ GeV}]$ | $7.29 \pm 0.05 \pm 0.30 \pm 0.00$ | $15.79 \pm 0.12 \pm 0.66 \pm 0.00$ |
| $R_{\text{QCD}} [1.8\text{--}3.7 \text{ GeV}]_{uds}$ | $33.45 \pm 0.28 \pm 0.59_{\text{dual}}$ | $24.27 \pm 0.18 \pm 0.26_{\text{dual}}$ |
| $R_{\text{QCD}} [5.0\text{--}9.3 \text{ GeV}]_{udsc}$ | 6.86 ± 0.04 | 34.89 ± 0.17 |
| $R_{\text{QCD}} [9.3\text{--}12.0 \text{ GeV}]_{udscb}$ | 1.21 ± 0.01 | 15.56 ± 0.04 |
| $R_{\text{QCD}} [12.0\text{--}40.0 \text{ GeV}]_{udscb}$ | 1.64 ± 0.00 | 77.94 ± 0.12 |
| $R_{\text{QCD}} [> 40.0 \text{ GeV}]_{udscb}$ | 0.16 ± 0.00 | 42.70 ± 0.06 |
| $R_{\text{QCD}} [> 40.0 \text{ GeV}]_t$ | 0.00 ± 0.00 | -0.72 ± 0.01 |
| Sum | $693.1 \pm 1.2 \pm 2.6 \pm 1.7 \pm 0.1_\psi \pm 0.7_{\text{QCD}}$ | $275.28 \pm 0.16 \pm 0.71 \pm 0.23 \pm 0.09_\psi \pm 0.55_{\text{QCD}}$ |

Table 1. Compilation of the contributions to $a_\mu^{\text{had,LO}}$ and $\Delta\alpha_{\text{had}}(m_Z^2)$ as obtained from HVPTools. Where three (or more) uncertainties are given, the first is statistical, the second channel-specific systematic, and the third common systematic, which is correlated with at least one other channel. For the contributions computed from QCD, only total uncertainties are given, which include effects from the α_s uncertainty, the truncation of the perturbative series at four loops, the FOPT vs. CIPT ambiguity, and quark mass uncertainties. Except for the latter uncertainty, all other uncertainties are taken to be fully correlated among the various energy regions where QCD is used. The additional uncertainty dubbed “dual” estimates possible quark-hadron duality violating effects in the QCD estimate between 1.8 and 2.0 GeV. The uncertainties in the Breit-Wigner integrals of the narrow resonances J/ψ and $\psi(2S)$ are dominated by the the respective electronic width measurements [58]. The uncertainties in the sums (last line) are obtained by quadratically adding all statistical and channel-specific systematic uncertainties, and by linearly adding correlated inter-channel systematic uncertainties.

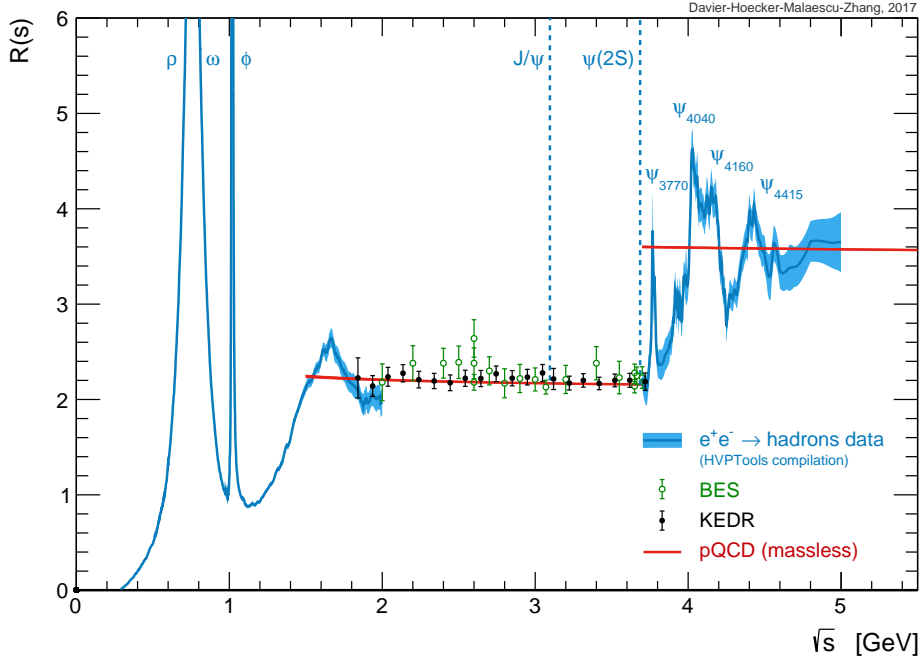


Fig. 10. The total hadronic e^+e^- annihilation rate R as a function of \sqrt{s} . Inclusive measurements from BES [42] and KEDR [43, 44] are shown as data points, while the sum of exclusive channels from this analysis is given by the narrow blue bands. Also shown is the prediction from massless perturbative QCD (solid red line).

that we use for this interval to avoid systematic effects due to possible unmeasured high-multiplicity channels.

Figure 10 shows the total hadronic e^+e^- annihilation rate R versus centre-of-mass energy as obtained from the sum of exclusive data below 2 GeV and from inclusive data between 1.8 and 5 GeV.⁶ Also indicated are the QCD prediction above 1.5 GeV and the analytical narrow J/ψ and $\psi(2S)$ resonances.

Muon magnetic anomaly

Adding all lowest-order hadronic contributions together gives

$$a_\mu^{\text{had,LO}} = 693.1 \pm 3.4, \quad (1)$$

which is dominated by experimental systematic uncertainties (cf. Table 1 for a separation of the total uncertainty into its components). The new result is 0.4 units larger than our previous evaluation [2] and 21% more precise owing to the new and improved experimental data.

Adding to (1) the contributions from higher order hadronic loops, -9.87 ± 0.09 (NLO) and 1.24 ± 0.01 (NNLO) [63], hadronic light-by-light scattering, 10.5 ± 2.6 [64], as well as QED, $11\,658\,471.895 \pm 0.008$ [65]

⁶ We have verified that the integration of the finely binned R distribution shown in Fig. 10, together with its covariance matrix, accurately reproduces the $a_\mu^{\text{had,LO}}$ and $\Delta\alpha_{\text{had}}(m_Z^2)$ results obtained by summing the exclusive modes below 1.8 GeV in Table 1.

(see also [60] and references therein), and electroweak effects, 15.36 ± 0.10 [66], we obtain the complete SM prediction

$$a_\mu^{\text{SM}} = 11\,659\,182.3 \pm 3.4 \pm 2.6 \pm 0.2 \quad (4.3_{\text{tot}}), \quad (2)$$

where the uncertainties account for lowest and higher order hadronic, and other contributions, respectively. The result (2) deviates from the experimental value, $a_\mu^{\text{exp}} = 11\,659\,209.1 \pm 5.4 \pm 3.3$ [59, 60], by 26.8 ± 7.6 (3.5σ).

A compilation of recent SM predictions for a_μ compared with the experimental result is given in Fig. 11.

Running electromagnetic coupling at m_Z^2

The sum of all quark-flavour terms from Table 1 gives for the hadronic contribution to the running of $\alpha(m_Z^2)$

$$\Delta\alpha_{\text{had}}(m_Z^2) = (275.3 \pm 0.9) \cdot 10^{-4}, \quad (3)$$

the uncertainty of which is dominated by data systematic effects ($0.7 \cdot 10^{-4}$) and the uncertainty in the QCD prediction ($0.6 \cdot 10^{-4}$).

Adding to (3) the three-loop leptonic contribution, $\Delta\alpha_{\text{lep}}(m_Z^2) = 314.97686 \cdot 10^{-4}$ [67], with negligible uncertainty, one finds

$$\alpha^{-1}(m_Z^2) = 128.947 \pm 0.012. \quad (4)$$

The current uncertainty on $\alpha(m_Z^2)$ is sub-dominant in the SM prediction of the W -boson mass (the dominant

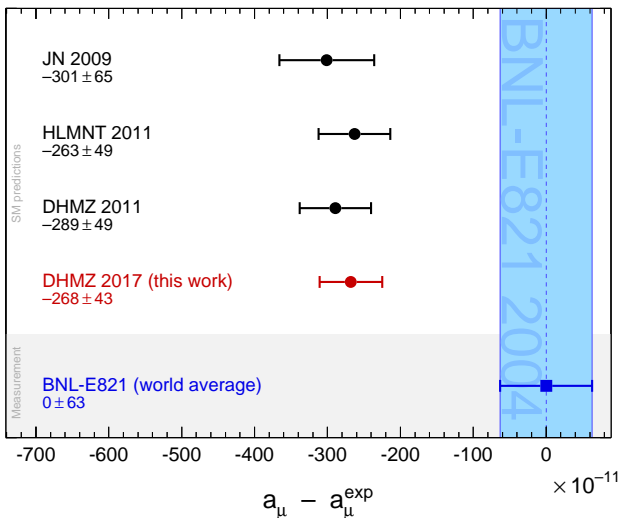


Fig. 11. Compilation of recent results for a_μ^{SM} (in units of 10^{-11}), subtracted by the central value of the experimental average [59, 60]. The shaded vertical band indicates the experimental uncertainty. The representative SM predictions are taken from this work (DHMZ 2017), DHMZ 2011 [2], HLMNT 2011 [61], and JN 2009 [62].

uncertainties are due to the top mass and of theoretical origin), but dominates the prediction of $\sin^2 \theta_{\text{eff}}^\ell$, which, however, is about twice more accurate than the combination of all present measurements [56].

4 Conclusions and perspectives

Using newest available $e^+e^- \rightarrow$ hadrons cross-section data we have reevaluated the lowest-order hadronic vacuum polarisation contribution to the Standard Model prediction of the anomalous magnetic moment of the muon, and the hadronic contribution to the running electromagnetic coupling strength at the Z -boson mass. For the former quantity we find $a_\mu^{\text{had,LO}} = (693.1 \pm 3.4) \cdot 10^{-10}$. The uncertainty of 0.5% on this contribution is now reduced to about half the current uncertainty of the a_μ measurement, and has improved by more than a factor of two during the last thirteen years. The discrepancy between measurement and complete Standard Model prediction remains at a non-conclusive 3.5σ level. The forthcoming experiments at Fermilab [68] and JPARC [69], aiming at up to four times better ultimate precision, have the potential to clarify the situation.

To match the precision of these experiments further progress is needed to reduce the uncertainty on $a_\mu^{\text{had,LO}}$ from dispersion relations. New analyses of the dominant $\pi^+\pi^-$ channel are underway at the BABAR and CMD3 experiments for which a systematic uncertainty of 0.3% may be reachable. In the 1–2 GeV range it is important to improve the precision of the $\pi^+\pi^-\pi^0$ and

K^+K^- channels. Independently of the data-driven approach, Lattice QCD calculations of $a_\mu^{\text{had,LO}}$ are also progressing albeit not yet reaching competitive precision [70].

The determination of $a_\mu^{\text{had,LO}}$ is closing in on the estimated uncertainty of the hadronic light-by-light scattering contribution $a_\mu^{\text{had,LBL}}$ of $2.6 \cdot 10^{-10}$, which appears irreducible at present. Here only phenomenological models have been used so far and Lattice QCD calculations could have a strong impact [71].

References

1. M. Davier, A. Hoecker, B. Malaescu, C.Z. Yuan, and Z. Zhang, Eur. Phys. J. C66, 1 (2010) [arXiv:0908.4300].
2. M. Davier, A. Hoecker, B. Malaescu, and Z. Zhang, Eur. Phys. J. C 71, 1515 (2011) [arXiv:1010.4180].
3. P.A. Baikov, K.G. Chetyrkin, and J.H. Kühn, Phys. Rev. Lett. 101, 012002 (2008) [arXiv:0801.1821].
4. BABAR Collaboration, Phys. Rev. Lett. 103, 231801 (2009) [arXiv:0908.3589].
5. BABAR Collaboration, Phys. Rev. D 86, 032013 (2012) [arXiv:1205.2228].
6. KLOE Collaboration, Phys. Lett. B 670, 285 (2009) [arXiv:0809.3950].
7. KLOE Collaboration, Phys. Lett. B 700, 102 (2011) [arXiv:1006.5313].
8. KLOE Collaboration, Phys. Lett. B 720, 336 (2013) [arXiv:1212.4524].
9. BESIII Collaboration, Phys. Lett. B 753, 629 (2015) [arXiv:1507.08188].
10. CMD2 Collaboration, Phys. Lett. B 578, 285 (2004) [hep-ex/0308008].
11. CMD2 Collaboration, JETP Lett. 82, 743 (2005) [hep-ex/0603021]; CMD2 Collaboration, JETP Lett. 84, 413 (2006) [hep-ex/0610016]; CMD2 Collaboration, Phys. Lett. B 648, 28 (2007) [hep-ex/0610021].
12. SND Collaboration, JETP Lett. 103, 380 (2006) [hep-ex/0605013].
13. M. Davier, A. Hoecker, B. Malaescu, C.Z. Yuan, and Z. Zhang, Eur. Phys. J. C 74, 2803 (2014) [arXiv:1312.1501].
14. F. Jegerlehner and R. Szafron, Eur. Phys. J. C 71, 1632 (2011) [arXiv:1101.2872].
15. K. Griessinger, (for the BABAR Collaboration), proceedings of the Tau Workshop, IHEP-Beijing (Sep. 2016).
16. BABAR Collaboration, Phys. Rev. D 85, 112009 (2012) [arXiv:1201.5677].
17. CMD3 Collaboration, Phys. Lett. B 768, 345 (2017) [arXiv:1612.04483].
18. BABAR Collaboration, Phys. Rev. D 89, 092002 (2014) [arXiv:1403.7593].
19. CMD3 Collaboration, Phys. Lett. B 760, 314 (2016) [arXiv:1604.02981].

20. SND Collaboration, Phys. Rev. D 94, 112006 (2016) [arXiv:1608.08757].
21. BABAR Collaboration, Phys. Rev. D 88, 032013 (2013) [arXiv:1306.3600].
22. CMD3 Collaboration, J. Univ. Sci. Tech. China 46, 507 (2016) [arXiv:1603.03230].
23. E.P. Solodov, private communication (2016).
24. M. Davier, S. Eidelman, A. Hoecker, and Z. Zhang, Eur. Phys. J. C 27, 497 (2003) [hep-ph/0208177]; Eur. Phys. J. C 31, 503 (2003) [hep-ph/0308213].
25. BABAR Collaboration, Phys. Rev. D 95, 052001 (2017) [arXiv:1701.08297].
26. BABAR Collaboration, arXiv:1704.05009 (2017).
27. BABAR Collaboration, Phys. Rev. D 86, 012008 (2012) [arXiv:1103.3001].
28. CMD3 Collaboration, Phys. Lett. B 756, 153 (2016) [arXiv:1510.00654].
29. CMD3 Collaboration, Phys. Lett. B 723, 82 (2013) [arXiv:1302.0053].
30. SND Collaboration, Phys. Rev. D 93, 092001 (2016) [arXiv:1601.08061].
31. SND Collaboration, Phys. Rev. D 90, 032002 (2014) [arXiv:1312.7078].
32. SND Collaboration, Phys. Rev. D 91, 052013 (2015) [arXiv:1412.1971].
33. SND Collaboration, Phys. Rev. D 88, 054013 (2013) [arXiv:1303.5198]; Phys. Rev. D 94, 112001 (2016) [arXiv:1610.00235].
34. SND Collaboration, Phys. Rev. D 94, 092002 (2016) [arXiv:1607.00371].
35. CMD3 Collaboration, arXiv:1706.06267 (2017).
36. BABAR Collaboration, Phys. Rev. D 91, 052013 (2015) [arXiv:1412.1971].
37. BABAR Collaboration, Phys. Rev. D 87, 092005 (2013) [arXiv:1302.0055].
38. CMD3 Collaboration, Phys. Lett. B 759, 634 (2016) [arXiv:1507.08013].
39. ADONE Collaboration, Nucl. Phys. B 517, 3 (1998).
40. SND Collaboration, Phys. Rev. D 90, 112007 (2014) [arXiv:1410.3188].
41. SND Collaboration, Phys. Rev. D 94, 032010 (2016) [arXiv:1606.06481].
42. BES Collaboration, Phys. Rev. Lett. 84, 594 (2000) [hep-ex/9908046]; Phys. Rev. Lett. 88, 101802 (2002) [hep-ex/0102003]; BES Collaboration, Phys. Lett. B 641, 145 (2006) [hep-ex/0605105]; Phys. Lett. B 677, 239 (2009) [arXiv:0903.0900].
43. KEDR Collaboration, Phys. Lett. B, 753, 533 (2016) [arXiv:1510.02667].
44. KEDR Collaboration, Phys. Lett. B 770, 174 (2017) [arXiv:1610.02827].
45. Crystal Ball Collaboration, Z. Phys. C 40, 49 (1988); Crystal Ball Collaboration, SLAC-PUB-5160 (1990).
46. A. Bäcker, Preprint DESY F33-77/03 (1977).
47. G. Bonneau and F. Martin, Nucl. Phys. B 27, 381 (1971).
48. M. Davier, S. Eidelman, A. Hoecker, and Z. Zhang, Eur. Phys. J. C 27, 497 (2003) [hep-ph/0208177].
49. BABAR Collaboration, Phys. Rev. D 95, 052001 (2017) [arXiv:1701.08297].
50. BABAR Collaboration, Phys. Rev. D 73, 052003 (2006) [hep-ex/0602006].
51. BESIII Collaboration, Phys. Lett. B 761, 98 (2016) [arXiv:1604.01924] (and references therein).
52. Particle Data Group, Chin. Phys. C 40, 100001 (2016), <http://pdglive.lbl.gov>.
53. P. Baikov, K.G. Chetyrkin, and J.H. Kühn, Phys. Rev. Lett. 101, 012002 (2008) [arXiv:0801.1821].
54. K.G. Chetyrkin, J.H. Kühn and M. Steinhauser, Nucl. Phys. B 482, 213 (1996) [hep-ph/9606230].
55. M. Davier and A. Hoecker, Phys. Lett. B 419, 419 (1998) [hep-ph/9801361].
56. Gfitter Group, Eur. Phys. J. C 74, 3046 (2014) [arXiv:1407.3792].
57. F. Le Diberder and A. Pich, Phys. Lett. B 286, 147 (1992).
58. Particle Data Group, J. Phys. G 37, 075021 (2010).
59. Muon $g-2$ Collaboration, Phys. Rev. D 73, 072003 (2006) [hep-ex/0602035].
60. A. Hoecker and W. Marciano, “The Muon Anomalous Magnetic Moment”, in: Review of Particle Physics, Physarticle Data Group, Chin. Phys. C, 40, 100001 (2016).
61. K. Hagiwara *et al.*, J. Phys. G 38, 085003 (2011) [arXiv:1105.3149].
62. F. Jegerlehner and A. Nyffeler, Phys. Rept. 477, 1 (2009) [arXiv:0902.3360].
63. A. Kurz *et al.*, EPJ Web Conf. 118, 01033 (2016) [arXiv:1511.08222].
64. J. Prades, E. de Rafael, and A. Vainshtein, Adv. Ser. Direct. High Energy Phys. 20, 303 (2009) [arXiv:0901.0306].
65. T. Aoyama, M. Hayakawa, T. Kinoshita, and M. Nio, Phys. Rev. Lett. 109, 111808 (2012) [arXiv:1205.5370].
66. C. Gnendiger, D. Stöckinger, and H. Stöckinger-Kim, Phys. Rev. D 88, 053005 (2013) [arXiv:1306.5546]; M. Knecht, S. Peris, M. Perrottet, and E. de Rafael, JHEP 0211, 003 (2002) [hep-ph/0205102]; A. Czarnecki, W.J. Marciano, and A. Vainshtein, Phys. Rev. D 67, 073006 (2003), Erratum-ibid. D 73, 119901 (2006) [hep-ph/0212229]; R. Jackiw and S. Weinberg, Phys. Rev. D 5, 2396 (1972).
67. M. Steinhauser, Phys. Lett. B 429, 158 (1998) [hep-ph/9803313].
68. Muon $g-2$ Collaboration, FERMILAB-FN-0992-E, FERMILAB-DESIGN-2014-02, arXiv:1501.06858 (2015).
69. E34 Muon $g-2$ /EDM experiment at JPARC, <http://g-2.kek.jp/portal/index.html>.
70. HPQCD Collaboration, arXiv:1601.03071 (2016); RBC and UKQCD Collaborations, Phys. Rev. Lett. 116, 232002 (2016) [arXiv:1512.09054]; T. Blum, Phys. Rev. Lett. 91, 052001 (2003).

71. T. Blum *et al.*, Phys. Rev. D 93, 014503 (2016) [arXiv:1510.07100].